

MIT Open Access Articles

*Effect of Operation Strategy on First Cycle CO,
HC, and PM/PN Emissions in a GDI Engine*

The MIT Faculty has made this article openly available. **Please share** how this access benefits you. Your story matters.

Citation: Rodriguez, J. Felipe, and Wai K. Cheng. "Effect of Operation Strategy on First Cycle CO, HC, and PM/PN Emissions in a GDI Engine." SAE Int. J. Engines 8, no. 3 (January 20, 2015).

As Published: <http://dx.doi.org/10.4271/2015-01-0887>

Publisher: SAE International

Persistent URL: <http://hdl.handle.net/1721.1/98049>

Version: Author's final manuscript: final author's manuscript post peer review, without publisher's formatting or copy editing

Terms of use: Creative Commons Attribution-Noncommercial-Share Alike



Effect of Operation Strategy on First Cycle CO, HC, and PM/PN Emissions in a GDI Engine

Author, co-author (Do NOT enter this information. It will be pulled from participant tab in MyTechZone)

Affiliation (Do NOT enter this information. It will be pulled from participant tab in MyTechZone)

Copyright © 2015 SAE International

Abstract

The impact of the operating strategy on emissions from the first combustion cycle during cranking was studied quantitatively in a production gasoline direct injection engine. A single injection early in the compression cycle after IVC gives the best tradeoff between HC, particulate mass (PM) and number (PN) emissions and net indicated effective pressure (NIMEP). Retarding the spark timing, it does not materially affect the HC emissions, but lowers the PM/PN emissions substantially. Increasing the injection pressure (at constant fuel mass) increases the NIMEP but also the PM/PN emissions.

Introduction

As a result of more stringent fuel economy standards aiming for CO₂ emissions of around 100gCO₂/km by 2025 [1], GDI engines have gained market penetration in the USA, with a 30% share of the gasoline engine sales in 2012 [2], and a prognosticated market share of up to 97% by 2025 [3]. GDI engines have better knock resistance through charge cooling; allow for aggressive scavenging to improve the low-end torque of turbo-charged engines and offer capability to increase the lean operation limit. On the other hand, liquid injection into the combustion chamber increases the emissions of unburned hydrocarbons (HC) and particulates (PM/PN), especially during cold-start. Figure 1 shows the normalized engine-out and tailpipe HC emissions during the FTP-75 for a gasoline engine. Due to the inactivity of the catalyst, more than 90% of the HC emissions occur during the first 2 minutes of operation.

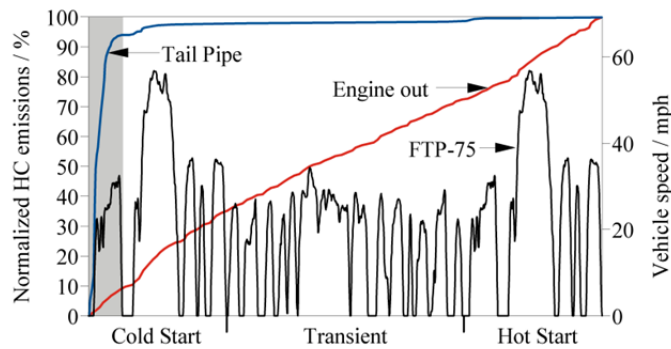


Figure 1. Cumulative engine-out and tailpipe HC emissions over the FTP-75 cycle for a gasoline engine.

In an effort to understand better the cold-start emissions, it is necessary to quantify the contribution of the cold crank-start process. Figure 2 shows the cumulative HC and PM emissions during the crank-start of a production GDI engine as a percentage of the maximum allowable emission limits for the U.S. standard T3B50 / ULEV50, assuming the same NMOG/NOx ratio as the T2B5 standard.

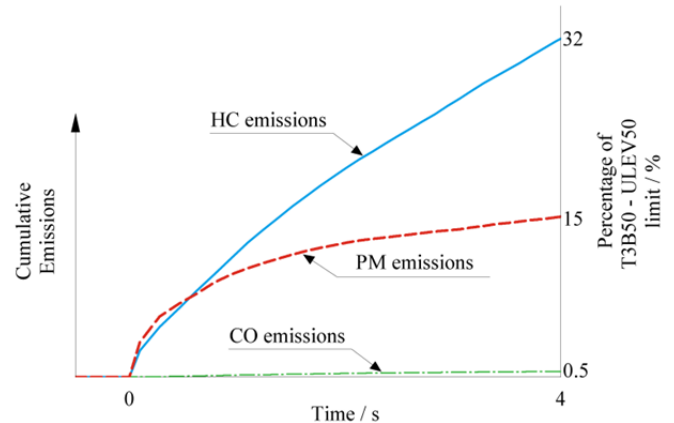


Figure 2. Cumulative emissions as percentage of the T3B50/ULEV50 limit

During a typical crank-start, the emissions account to 110 mg of unburned HC corresponding to 32% of the T3B50 limit and 5 mg of particulates corresponding to 15% of the T3B50. Additionally, the number of particles emitted are 2.7×10^{12} corresponding to 40% of the Euro6 limit (U.S. regulations do not include a limit for the number of particles). Given the significant impact of the cold cranking process in the overall emissions, it is necessary to gain a better understanding of the formation mechanism of the pollutants during engine crank-start and their dependence to the injection strategy during cranking.

The cold wall temperature and low engine speed during the crank-start process pose significant constraints on the mixture formation process. The cold cylinder walls result in the formation of fuel films which, in turn, are partly responsible for the high levels of HC and PM/PN emissions. Additionally, the cold temperature promotes the absorption of fuel into the oil layer prior to combustion. After combustion, the hot burned gas with low HC concentration favors desorption of the fuel back into the bulk gases, providing an additional source for HC emissions. The low wall temperature also results in increased heat transfer away from the flame front during combustion causing a larger flame quenching distance, increasing the

amount of gaseous fuel escaping combustion. Finally, the post-flame oxidation rate of the HC that managed to escape combustion and of the particles formed during combustion is reduced due to increased heat transfer to the cold cylinder walls.

The low engine speed impacts the degree of charge motion during cranking. This results in poor mixture formation, in the form of reduced evaporation of the fuel and reduced homogeneity of the mixture. Additionally, the post-flame oxidation is affected by the mixing process of the unburned HC layer in the vicinity of the walls with the hot bulk gases. This mixing process is a function of engine speed and it is negatively impacted during crank-start.

The cold cranking process for GDI engines has been studied experimentally and numerically in the past. Fan et al. studied experimentally the effect of split injection on the combustion characteristics of the first cycle [4] and on the HC emissions behavior of the complete cranking process [5]. Whitaker et al. [6] studied in an optical engine the effect of fuel pressure on spray penetration and droplet size at cranking speed as well its effect of PM emissions. Geringer et al. [7] studied the startability at extreme cold temperatures using E85, and the effect of throttling on the evaporation of the fuel and the run-up time. Wiemer et al. [8] measured the effect of fuel quantity, injection timing and spark timing on the run-up speed trace and HC emissions.

Using CFD analysis Kim et al [9] studied the AFR distribution during cranking at subzero conditions for different injection timings. Similarly, Malaguti et al. performed numerical analysis for the first [10] and second [11] combustion cycles, focusing on spray-wall interaction and its effect in fuel evaporation and liquid fuel film formation. Also, Xu et al. [12] modeled the engine cranking and run-up for split injection strategies and their impact on the AFR around the spark plug.

This paper also builds upon the methodology developed at MIT for studying the first combustion cycle and the cranking process in PFI-SI engines [13 - 18].

Of all the cycles during the engine crank-start, the first combustion event is the most problematic since it experiences the lowest temperature and engine speed. Additionally, the absence of hot residual gases reduces the evaporation of the fuel spray compared to the next combustion cycles during crank-start. The goal of this study is to quantify the individual contributions of a broad set of different variables affecting the mixture formation process, and their impact on the combustion behavior and on the emissions of CO, HC and PM for that first combustion event during cranking.

Experimental Methodology

Engine set up

The experiments were carried out in a GM LNF engine; with the specifications given in Table 1. The engine features a centrally mounted spark plug and 4 valves per cylinder. The valve timing corresponds to the parked position of the camshafts, resulting in a negative valve overlap of 20°CA. This valve timing reduces the volumetric efficiency and effective compression ratio and increases the residual gas fraction during the cranking process. The injection

system (Fig. 3) consists of side-mounted, 6-hole electromagnetic injectors with a horizontal inclination of 47° and a cone angle of 52°.

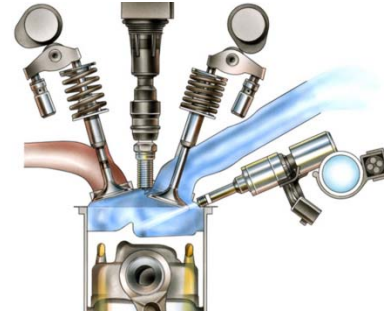


Figure 3. Combustion system of GM's LNF engine ©GM

Table 1. Engine specifications

Displacement	1998 cc
Bore / Stroke	86 / 86 mm
Connecting Rod	145.5 mm
Compression ratio	9.2:1
Inlet Valve Open / Close	11°aTDC / 61°aBDC @ 0.2 mm lift
Max. intake valve lift	10.3 mm @ 126°aTDC
Exhaust Valve Open / Close	52°bBDC / 10°bTDC @ 0.2 mm lift
Max. exhaust valve lift	10.3 mm @ 125°aTDC

The fuel, intake air and coolant temperature are kept at 20°C. The fuel is pressurized by a hydro-pneumatic accumulator using high pressure nitrogen, allowing the fuel pressure to be set independently from engine operation. The fuel used is a Tier II EEE certification gasoline with a carbon mass fraction of 86.5%.

The exhaust composition is measured using fast response analyzers from Cambustion. The HC concentration is measured using an FFID unit (HFR400), with a response time t_{10-90} of 1ms, and a sampling position 6cm from the exhaust valve. The CO and CO₂ concentrations are measured with a fast NDIR unit (NDIR500), with a response time t_{10-90} of 8ms, and a sampling position 8cm from the exhaust valve. The PM and PN are measured using a fast particle spectrometer (DMS500) with a t_{10-90} of 300ms a sampling point 15cm from the exhaust valve.

The DMS500 classifies particles in a discrete manner based on their electrical mobility, i.e. their drag to charge ratio. A typical particle concentration vs. size spectrum is shown in Figure 4. The discrete measurement is fitted by two lognormal distributions, corresponding to the nucleation mode and to the accumulation mode. The lognormal distribution provides the best empirical fit in aerosol statistics. The distribution is described by the geometric standard deviation and the geometric mean of the diameters, which due to the symmetry of the distribution also corresponds to the median. In aerosol characterization, that median receives the name of count median diameter (CMD, see Fig. 4).

Since the European Particle Measurement Program (PMP) requires the removal of the volatile fraction, and given the low contribution of volatile particles to PM, it was chosen to consider the accumulation mode exclusively. In addition the sampling temperature was kept at 150°C to prevent volatiles condensation on the accumulation mode.

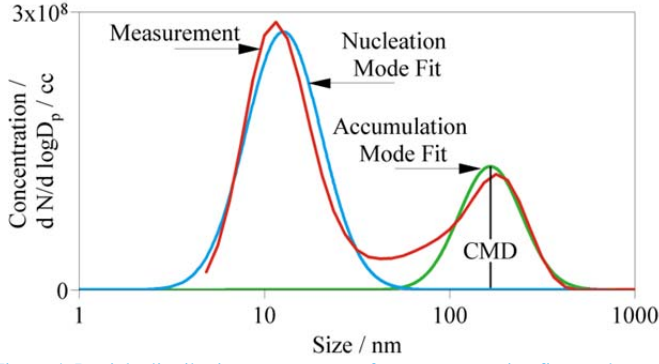


Figure 4. Particle distribution measurement for a representative first cycle

Experiment description

The experiment carried out to study the first cycle emissions during the crank-start process is presented in Figure 5. In order to recreate the conditions at cold cranking, the engine coolant, fuel and intake air temperatures are kept at 20°C. The experiment starts with the engine being motored at a cranking speed of 280 rpm for several cycles in order to evacuate the residual HC stored in the combustion chamber and to measure the HC background concentration. Then a metered amount of Tier II EEE certification gasoline is injected followed by a combustion event. The engine continues to be motored for 50 additional engine cycles at 280 rpm, while the HC, CO, CO₂ and PN concentrations are measured and recorded throughout the process.

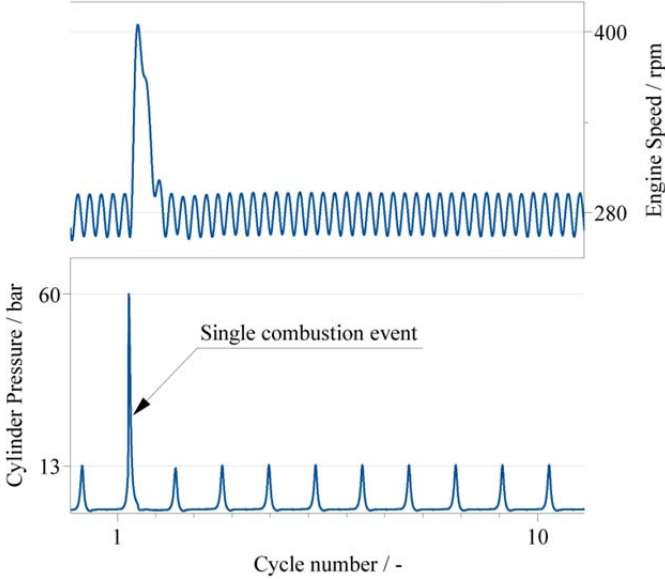


Figure 5. Engine speed and cylinder pressure during the single fire experiment

To assess the impact of the first cycle emissions it is necessary to translate the concentration measurements to exhausted mass of pollutants. To achieve this, further information about the exhaust mass flow rate is required. This information can be extracted from the cylinder pressure trace and the piston position by idealizing the exhaust process as an isentropic expansion of an ideal gas as shown in Eq. 1.

$$\dot{m}_{exh} = - \left(\frac{1}{\gamma P_{cyl}} \frac{dP_{cyl}}{dt} + \frac{1}{V_{cyl}} \frac{dV_{cyl}}{dt} \right) m_{cyl} \quad (1)$$

Figure 6 shows two typical mass flow rate traces for a fired and a motored exhaust stroke. Both traces have opposite behaviors between EVO and BDC. The fired cycle displays a blowdown process as the exhaust valve opens, while a reverse flow occurs for the motored cycle. In order to account for this difference, the phasing of concentration signals is corrected considering the velocity of the exhaust gas inside the runner. Then, the corrected signal is integrated over the exhaust event as shown in Eq. 2.

$$m_{k,cycle} = \int_{t_{EVO}}^{t_{EVC}} \hat{x}_k(t + \tau(t)) \frac{M_k}{M_{exh}} \frac{dm_{exh}}{dt} dt \quad (2)$$

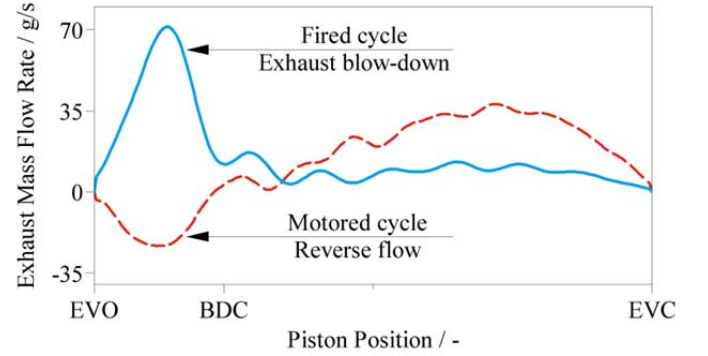


Figure 6. Mass flow rates for fired and motored exhaust events

The concentration of number of particles per standard cubic centimeter (#/scc) can be found by integrating the lognormal distribution for the accumulation mode (see Fig. 4 and Eq. 3). The total number of particles can be calculated by integrating the product of particle concentration with the standard volumetric exhaust flow (Eq. 3).

$$\hat{N} \left[\frac{\#}{scc} \right] = \int_{1 \text{ nm}}^{1000 \text{ nm}} \frac{dN}{d \log D_p} d \log D_p \quad (3)$$

$$PN[\#] = \int_{t_{EVO}}^{t_{EVC}} \hat{N} \frac{1}{\rho_{std}} \frac{dm_{exh}}{dt} dt$$

The calculation of the PM from the PN and size spectrum measurement requires additional consideration of the morphology of the soot particles and of their specific gravity. For GDI engines the recommended fractal dimension $D_f=3$ (so that volume is proportional to d^{D_f}), i.e. spherical particles, and the recommended specific gravity is 1 [19]. The total mass can be found by weighting the lognormal distribution with the particle density and multiplying by the standard volumetric exhaust flow (Eq. 4).

$$\hat{M} \left[\frac{\mu g}{scc} \right] = \int_{1 \text{ nm}}^{1000 \text{ nm}} (5.2 \times 10^{-16} D_p^3) \frac{dN}{d \log D_p} d \log D_p \quad (4)$$

$$PM[\mu g] = \int_{t_{EVO}}^{t_{EVC}} \hat{M} \frac{1}{\rho_{std}} \frac{dm_{exh}}{dt} dt$$

Results

A number of variables influence the mixture formation process and the emissions behavior of the first firing cycle during the cranking process. This study focuses on the four most relevant injection parameters using a one-variable-at-a-time approach. The variables studied are: Start of injection (SOI), fuel enrichment factor (FEF), ignition timing, and fuel pressure. The swept ranges and the nominal points are presented in Table 2. Unless otherwise stated, all the variables stay constant at the nominal values during the different sweeps.

Table 2. Experimental matrix

Variable	Sweep range	Nominal value
Start of injection	30 to 315 °aTDC-i	90 °aTDC-i
FEF	1.7 to 3.5	2.5
Ignition timing	-45 to 20 °aTDC-c	-10 °aTDC-c
Fuel pressure	30 to 110 bar	50 bar

The FEF quantifies the amount of fuel injected in comparison to the amount of fuel required to achieve stoichiometric operation during steady state cold idle operation (Eq. 5). At nominal conditions (see Table 2), an FEF=1 corresponds to 29.5 mg of fuel. The volumetric efficiency during cranking (280 rpm, valve timing fixed) is 80%.

$$FEF = \frac{m_{f,cyl}}{V_{cyl} \cdot \eta_{vol} \cdot \rho_{int} \cdot (F/A)_{stoich}} \quad (5)$$

Start of Injection and Fuel Enrichment Factor

The two most important variables affecting the mixture formation and the combustion and emissions behavior are the SOI and the FEF. Figure 7 shows the dependence of the NIMEP, CO and HC emissions on the SOI, while keeping the rest of the variables at the nominal values shown in Table 2.

Due to the interaction of the spray with the piston at very early injections (SOI=<30°aTDC-i) the engine misfires as can be read from the negative NIMEP (Fig. 7 top), and from the high relative HC emissions. For SOI between 45 to 75°aTDC-i, significant wetting of the piston is avoided and the relative HC emissions are reduced to 2-3% while the NIMEP increases from 4 to 6 bar.

For the SOI range from 90 to 180°aTDC-i the relative HC emissions increase to a peak value of 4.5% and then decrease again to 2%, most likely due to spray interaction with the intake valve. As the valve recedes into its seat during the early part of the compression stroke, a SOI ranging from 180 to 225°aTDC-i results in consistently lower relative HC emissions at 2% while the NIMEP increases from 5.5 to 6.8 bar, suggesting better mixture formation. Lastly, for injection during the late compression stroke (SOI=240 to 315°aTDC-i) the relative HC and CO emissions increase significantly, while the NIMEP goes down slightly. At this late SOI, the interaction between the injection spray and the piston promotes the formation of fuel films on the piston crown, as well as an overly enriched air-fuel mixture around the sparkplug.

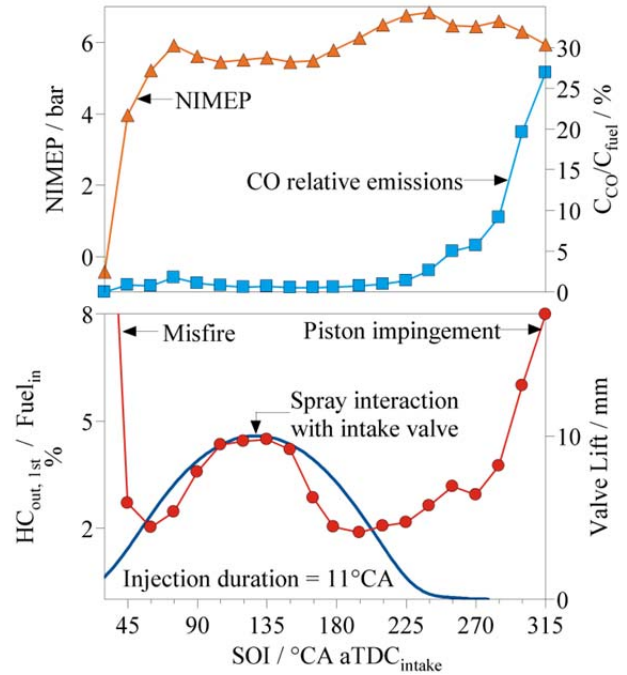


Figure 7. First cycle NIMEP, CO and HC emissions as a function of the SOI

The PM/PN emissions (Fig. 8) exhibit some similarities to the HC emissions (Fig. 7), especially for SOI during the compression stroke. For SOI during the intake stroke, the soot emissions decrease monotonically to a minimum of 30µg and 10¹⁰ number of particles. The count median diameter (CMD) of the particles also reduces slightly from 150nm to 140nm. The interaction of the fuel spray with the intake valve has no noticeable effect, and the trends are dominated by the interaction with the piston. As the SOI moves into the compression stroke, the particle emissions increase significantly, both in number and size, reaching 1.6x10¹¹ and 168nm respectively, corresponding to a PM emission of 800µg.

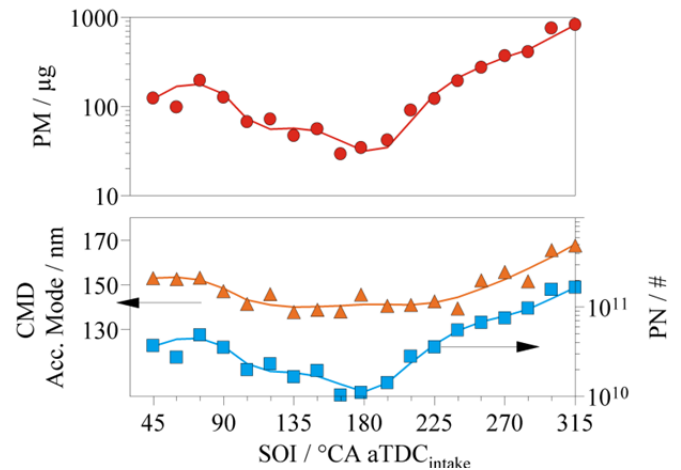


Figure 8. First cycle PM/PN emissions and average particle size as a function of the SOI

It is desirable for cold transient management to maximize the work output while at the same time minimize the pollutant emissions. In this regard, the crank-start process is no different. Figure 9 (top) presents the 1st cycle NIMEP as a function of the FEF for 4 different injection timings. The respective tradeoffs between NIMEP and pollutant emissions are presented in Fig. 9 for CO and HC (middle and bottom) and in Fig. 10 for PM/PN.

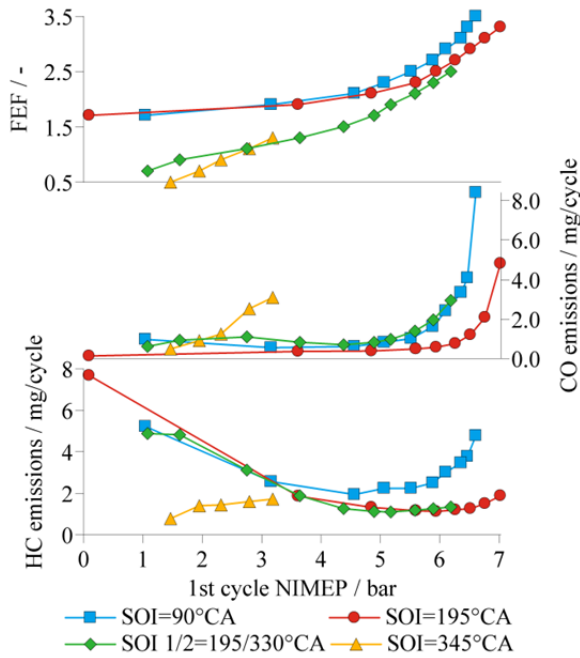


Figure 9. Effect of FEF on NIMEP, CO, and HC emissions for the 1st cycle

Four different injection strategies were selected for the FEF sweep:

1. Injection during intake valve opening (SOI=90° aTDC-i).
2. Early compression stroke injection (SOI=195° aTDC-i).
3. Split injection with a fixed second injection mass at 6mg (SOI 1/2=195/330° CA). (As a reference, at FEF = 1, the total fuel was 29.5 mg.)
4. Late compression stroke injection (SOI=345° aTDC-i).

In general, the NIMEP increases monotonically with FEF, with a reduced trend when the mixture becomes overly enriched around the sparkplug, as can be inferred from the increasing partial oxidation of fuel to CO (Fig. 9). The late injection strategy (SOI=345° aTDC-i) reduces the FEF requirement for avoiding a partial burn or a misfire, while keeping the HC emissions at a low level. On the other hand, the soot emissions (Fig. 10) increase dramatically in number and size even at low NIMEP, making this injection strategy unattractive.

The injection strategy during intake valve opening (SOI=90° aTDC-i) results in the highest HC emissions and increased FEF requirement for a given NIMEP (Fig 9). The soot emissions are also deteriorated in comparison to a closed valve injection, with PM emissions up to an order of magnitude higher.

A common strategy used by OEMs during engine crank-start is the so called high-pressure stratified start [20, 21, 22]. The split injection strategy used in this study aims to reproduce such approach. The injection of a small amount of fuel late in the compression stroke reduces the FEF requirement for a given NIMEP, by creating a stratified mixture around the sparkplug as can be seen from the increased amount of CO in comparison to a single injection at SOI=195° aTDC-i. Additionally, the HC emissions for a given NIMEP are at the same level of the single injection at SOI=195° aTDC-i, suggesting that the reduction in FEF compensates for the increase in piston impingement (Fig 9, bottom). Although the piston interaction has a negligible effect in the HC emissions, its

effect on the PM/PN emissions (Fig. 10) is significant, increasing the soot mass emissions up to an order of magnitude, achieving similar values as the open valve injection strategy.

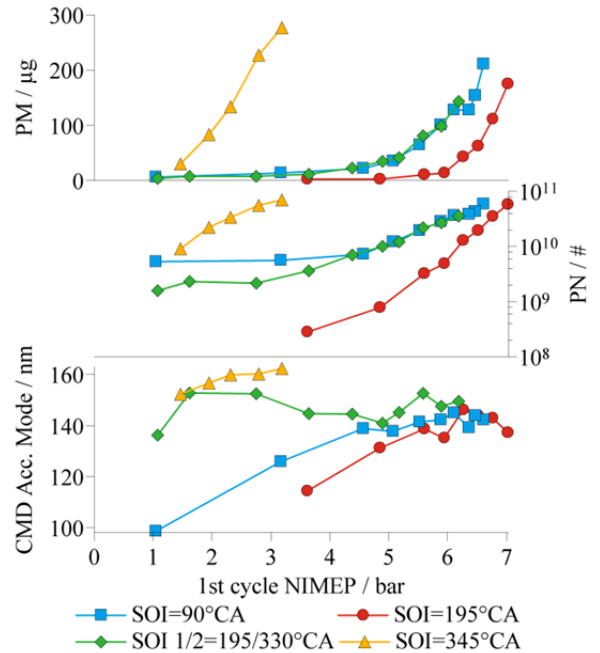


Figure 10. Effect of FEF on PM/PN emissions and average particle size for the 1st cycle

Lastly, the single injection during the early compression stroke (SOI=195° aTDC-i) results in the most favorable injection strategy in terms of pollutant emissions for a given NIMEP, if the risk of partial burn or misfire is correctly managed by adjusting the minimum FEF appropriately.

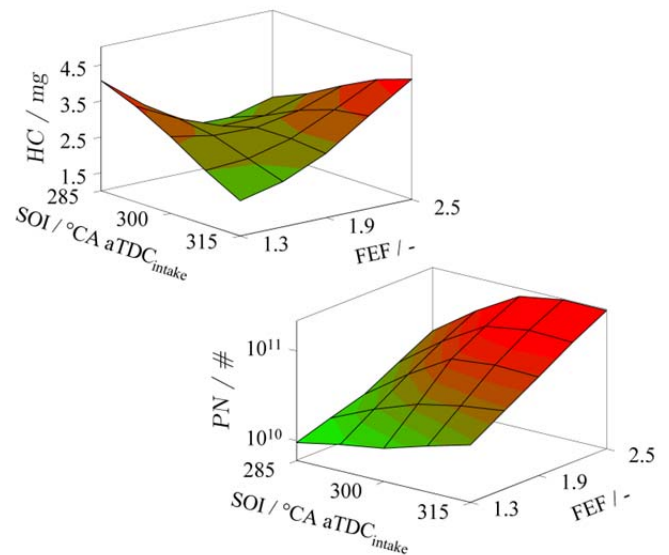


Figure 11. HC and PN dependence on SOI and FEF for the 1st cycle

In summary, in comparison to the early compression stroke single injection strategy (SOI=195° aTDC-i), the open valve injection results in increased HC and PM emissions. Late compression injection increases the combustion robustness at the cost of inadmissibly high

PM emissions. The split injection, or high high-pressure stratified start strategy, increases the combustion robustness and achieves the same HC emissions performance, but increases the PM emissions. As shown in Fig. 11, the increased stratification achieved at later injection timings can improve the HC emissions at low FEF as a consequence of faster burn rates reducing the partial burn. At higher FEF, when partial burn is no longer a concern, later SOI results in higher HC emissions. However, the dependence of PN on SOI and FEF for compression injection is monotonic. Later SOI and higher FEF result invariably in higher soot emissions (Fig. 11).

The effect of the FEF on the combustion phasing can be seen in Fig. 12. Open valve injection results in the highest sensitivity of the mass fraction burned (MFB) to FEF. As injection is delayed to the early compression stroke, the sensitivity is reduced. Further reduction is achieved by the split injection strategy, achieving a constant CA10 and CA50, with CA90 remaining a function of FEF. In the case of very late single injection, the dependence of combustion phasing to FEF disappears.

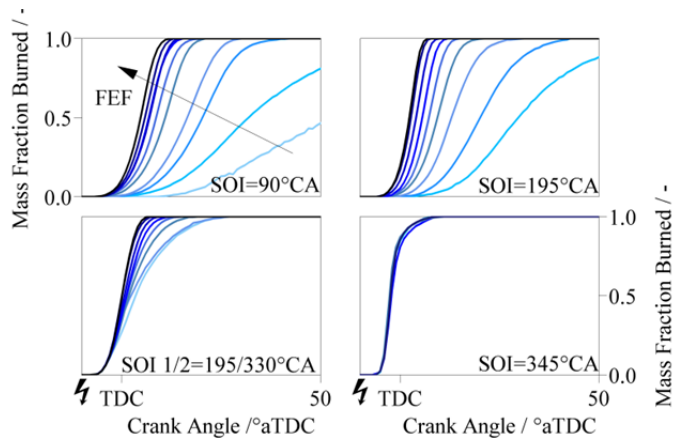


Figure 12. Effect of the FEF on the combustion phasing for 4 different injection strategies. The FEF range for each case can be found in Figure 9 (top).

Ignition Timing

A well-known strategy for the reduction of engine-out HC emissions and fast catalyst warm-up during steady state operation consists of retarding of the spark timing [23, 24, 25]. Given the unique characteristics of the first combustion cycle, there was interest to examine whether this strategy was also applicable.

Figure 13 shows the relative HC emissions as a function of the ignition timing for two different injection timings (SOI=90°aTDC-i and SOI=195°aTDC-i), all other parameters remaining constant at their nominal value. The ignition timing was varied from -45°aTDC-c to 20°aTDC-c. In the case of open valve injection, advanced ignition results in higher relative HC emissions at 3.8%. The retarding of the ignition timing to 2°aTDC-c results in a HC emissions reduction to 2.7% (~0.75mg reduction). Further spark retard does not lead to an additional benefit, but does result in a sharp decrease in NIMEP. In the case of early compression injection, the relative HC emissions are insensitive to spark timing, remaining constant at approximately 2% (~1.5mg), and exhibiting a slight increase for very late ignition. Higher CO emissions for advanced ignition timings can be observed for both injection strategies (Fig. 13, middle). Advanced ignition results in higher unburned gas temperatures in the fresh mixture ahead of the flame front. This

promotes the evaporation of the fuel films on the cylinder walls, leading to the formation of a richer mixture for the last gas elements participating in combustion, increasing the formation of CO and CO₂ [26].

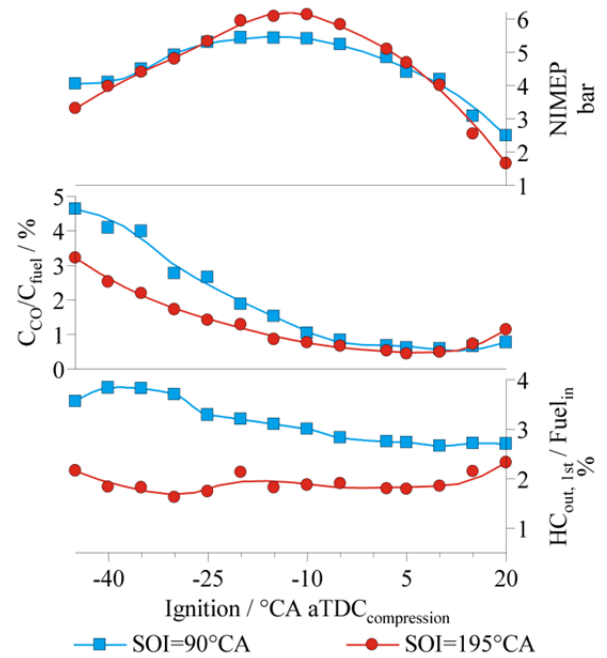


Figure 13. Effect of spark timing on 1st cycle NIMEP, CO and HC emissions

Conversely, the particulate emissions are very sensitive to the spark timing as can be seen in Fig.14. In the case of early injection timing (SOI=90°aTDC-i), the retard in spark timing from -45°aTDC-c to 20°aTDC-c, results in a PM reduction of an order on magnitude. This result is driven by both a reduction in PN, as well as by a reduction in particle size (165nm at -45°aTDC-c to 75nm at 20°aTDC-c).

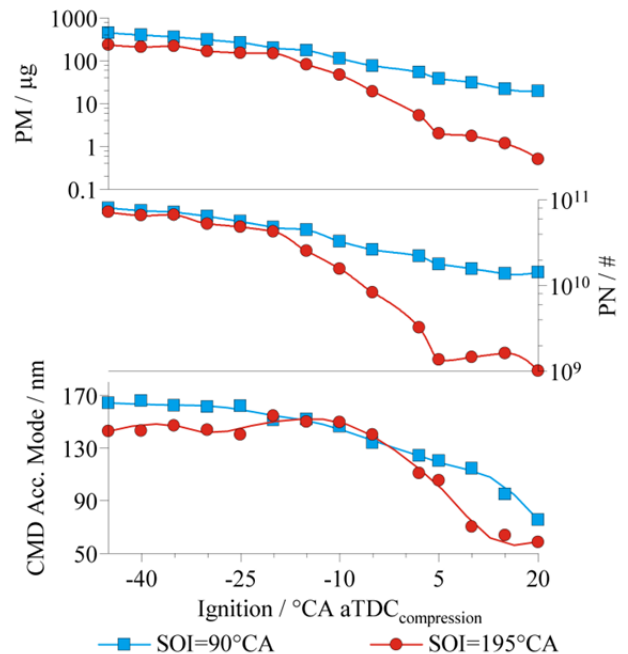


Figure 14. Effect of spark timing on 1st cycle PM/PN emissions

In the case of early compression injection (SOI=195°aTDC-i), the reduction in PM with spark timing is even more significant covering almost 3 orders of magnitude (230µg at -45°aTDC-c to 0.5µg at 20°aTDC-c). The result is mainly driven by the PN emissions up to TDC ignition timing. Further spark retard from this point results in no advantage in the PN emissions (constant at 10⁹), but does affect the particle size with a 50% reduction (110nm at 2°aTDC-c to 58nm at 20°aTDC-c).

In normal engine operation, substantial reduction in HC is observed with spark retard, which increases the charge temperature in the later part of the expansion process and facilitates the secondary oxidation of the crevice HC, which is a major source [27, 28]. In the first cycle of the cranking process, however, the major HC source is the fuel vapor from the fuel film on the cylinder surfaces. The amount of HC is substantial, and, unlike the crevice HC, it is not premixed with air. Thus the amount of HC that gets oxidized is small compared to the total amount. Therefore the HC emissions are not sensitive to the extent of secondary oxidation. Hence, the spark timing, which influences the secondary oxidation, does not materially affects the HC emissions.

For the PM emission, the formation of the particulates is a result of the post-flame pyrolysis of the rich unburned mixture formed from the fuel vapor that evaporates from the in-cylinder liquid fuel film [29]. With spark retard, the flame arrives at the cylinder wall later; thus the pyrolysis time is reduced, thereby reducing both the amount of particle formation and growth.

Fuel Pressure

The injection pressure has a direct influence in the mixture formation process due to its impact in fuel droplet size and momentum, thereby affecting the evaporation, wall wetting and charge turbulence. Emissions performance and combustion behavior of current GDI injection systems benefit from increased injection pressures, with 200 bar being today's standard pressure [30]. During engine cranking the fuel pressure must increase from around 5 bar (low pressure pump) to the targeted first cycle injection pressure. The pressure build-up is a function of the cranking time before first cycle combustion and the cranking speed. A typical first cycle fuel pressure lies between 30-50 bar [31]. This section concerns itself with the effect of increasing the first cycle fuel pressure on the HC and PM/PN emissions.

The same two injection strategies were examined, SOI=90°aTDC-i and SOI=195°aTDC-i while keeping constant the amount of fuel injected and keeping all other parameters at their nominal value. The results are shown in Figs. 15 and 16.

Higher fuel pressure results in better mixture formation as can be inferred from the increasing NIMEP (Fig. 15, top). The CO emissions were insensitive for the case of SOI=195°aTDC-i, while they increased with at higher fuel pressures for the injection timing SOI=90°aTDC-i due to interaction of the spray with the intake valve. A similar observation was made for the relative HC emissions; insensitive when SOI=195°aTDC-i, and a slight increase with fuel pressure at SOI=90°aTDC-i (Fig. 15, bottom).

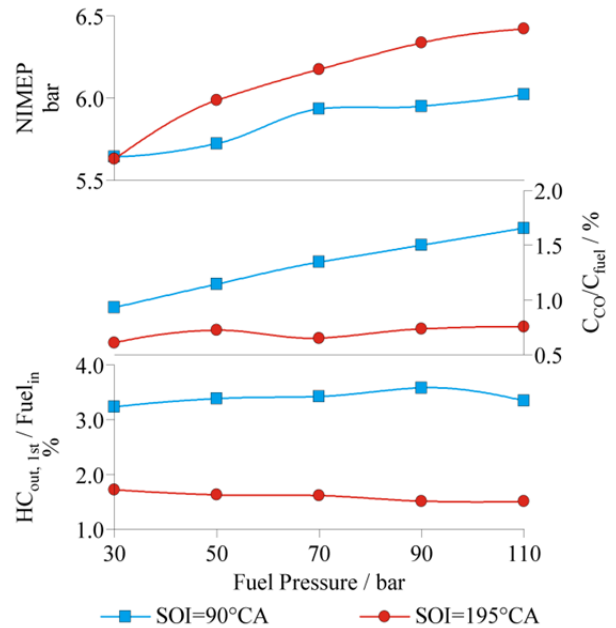


Figure 15. Effect of fuel pressure on 1st cycle NIMEP, CO and HC emissions. The fuel amount was kept constant

As has been already observed during the other parameter sweeps, PM/PN emissions have a higher sensitivity to the injection strategy, in this case to fuel pressure. At SOI=90°aTDC-i, the PM emissions increase 2.5 times going from 100µg at 30 bar to 250µg at 110 bar. For the injection timing SOI=195°aTDC-i, the relative increase is more substantial going from 14µg to 67µg in the same range. In both cases the increase in PM was driven by an increase in PN, since the fuel pressure showed no effect on the particles median size (Fig. 16).

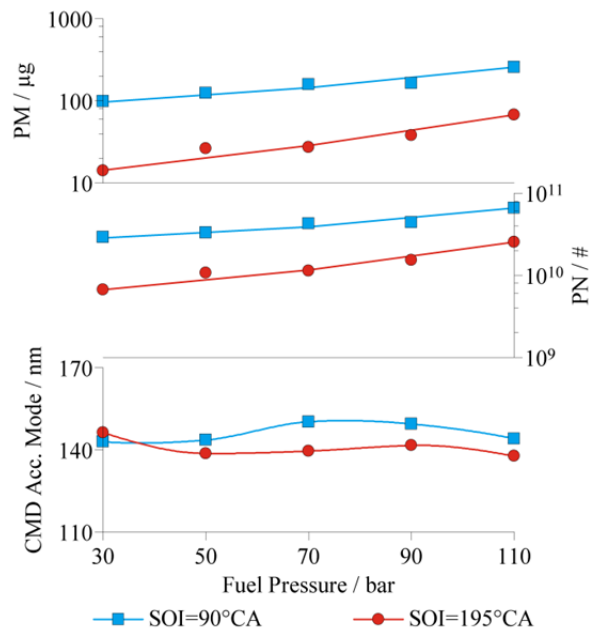


Figure 16. Effect of fuel pressure on 1st cycle PM/PN emissions

In summary, increasing the first cycle fuel pressure from the levels found in today's GDI engines results in a modest first cycle NIMEP benefit, which is more than offset by the worse performance in PM/PN emissions. The HC emissions are not sensitive to the fuel pressure.

Summary/Conclusions

The effects of four different engine operating parameters for the first combustion cycle during cranking were studied in a wall guided gasoline direct injection engine. The parameters examined were the injection timing, fuel enrichment, spark timing, and fuel pressure. The effects were assessed in terms of work output, CO, HC, and PM/PN emissions. An optimal first cycle operating strategy can be built upon the following key findings:

1. A single injection during the early compression stroke after IVC results in the best emissions behavior without decreasing the work output.
2. When compared to the early compression stroke single injection strategy in (1), a split injection strategy with a small amount of fuel (~20% of total) injected close to TDC- compression increases the combustion robustness, decreases the fuel enrichment requirement, achieves the same HC emissions performance, but increases the PM/PN emissions up to an order of magnitude.
3. In comparison to early compression stroke injection after IVC, open valve injection results in increased HC and PM emissions due to interaction of the fuel spray with the intake valve.
4. Injection late in the compression stroke increases the combustion robustness, decreases the fuel enrichment requirement, but results in inadmissibly high PM/PN emissions.
5. Delaying the spark timing up to TDC results in significant reduction of the PM/PN emissions, without a significant decrease in work output. The HC emissions, on the other hand, are insensitive to the spark timing. Further spark retard from TDC further reduces the PM/PN emissions, but with the penalty of decreasing the NIMEP.
6. Increasing the fuel pressure from 30 to 110 bar (while keeping the fuel amount the same) results in rising PM/PN emissions but better work output. The HC emissions are not sensitive to fuel pressure.

References

1. Façanha, Cristiano, Kate Blumber, and Josh Miller. Global Transportation Energy and Climate Roadmap. International Council on Clean Transportation, 2012.
2. He, Hui, and Anup Bandivadekar. "Passenger Car Fuel-Efficiency Standards in China and the US: Stringency and Technology, 2020–2025." International Council on Clean Transportation, 2013.
3. EPA; NHTSA. "Final Rulemaking for 2017-2025 Light-Duty Vehicle Greenhouse Gas Emission Standards and Corporate Average Fuel Economy Standards." 2012.
4. Fan, Q., J. Bian, H. Lu, L. Li, and J. Deng. "Effect of the Fuel Injection Strategy on First-Cycle Firing and Combustion Characteristics during Cold Start in a TSDI Gasoline Engine." International Journal of Automotive Technology 13 (4): 523–31. doi:10.1007/s12239-012-0050-3.
5. Fan, Q. and Li, L., "Transient Characteristics of Cold Start Emissions from a Two-Stage Direct Injection Gasoline Engines Employing the Total Stoichiometric Ratio and Local Rich Mixture Start-up Strategy," SAE Technical Paper 2012-01-1068, 2012, doi:10.4271/2012-01-1068.
6. Whitaker, P., Kapus, P., Ogris, M., and Hollerer, P., "Measures to Reduce Particulate Emissions from Gasoline DI engines," SAE Int. J. Engines 4(1):1498-1512, 2011, doi:10.4271/2011-01-1219.
7. Geringer, Bernhard, Peter Hofmann, and Florian Holub. 2010. "Verbesserung des Hochlaufs und des Emissionsverhaltens im Kaltstart und Warmlauf bei Ottomotoren." MTZ - Motortechnische Zeitschrift 71 (5): 368–72. doi:10.1007/BF03225576.
8. Wiemer, S., Kubach, H., and Spicher, U., "Investigations on the Start-Up Process of a DISI Engine," SAE Technical Paper 2007-01-4012, 2007, doi:10.4271/2007-01-4012.
9. Kim, S., Hyun, S., and Park, J., "Optimization of Cold Start Operating Conditions in a Stoichiometric GDI Engine with Wall-guided Piston using CFD Analysis," SAE Technical Paper 2013-01-2650, 2013, doi:10.4271/2013-01-2650.
10. Malaguti, S., Cantore, G., Fontanesi, S., Lupi, R. et al., "CFD Investigation of Wall Wetting in a GDI Engine under Low Temperature Cranking Operations," SAE Technical Paper 2009-01-0704, 2009, doi:10.4271/2009-01-0704.
11. Malaguti, S., Fontanesi, S., and Severi, E., "Numerical Analysis of GDI Engine Cold-Start at Low Ambient Temperatures," SAE Technical Paper 2010-01-2123, 2010, doi:10.4271/2010-01-2123.
12. Xu, Z., Yi, J., Wooldridge, S., Reiche, D. et al., "Modeling the Cold Start of the Ford 3.5L V6 EcoBoost Engine," SAE Int. J. Engines 2(1):1367-1387, 2009, doi:10.4271/2009-01-1493.
13. Lang, K. and Cheng, W., "Effect of Fuel Properties on First Cycle Fuel Delivery in a SI Engine," SAE Technical Paper 2004-01-3057, 2004, doi:10.4271/2004-01-3057.
14. Lang, K., Cheng, W., Borland, M., Thomas, C. et al., "Effect of Intake Cam Phasing on First Cycle Fuel Delivery and HC Emissions in an SI Engine," SAE Technical Paper 2004-01-1852, 2004, doi:10.4271/2004-01-1852.
15. Cowart, J., "Air-Fuel Ratio Measurement Diagnostics During Cranking and Startup in a Port-Fuel-Injected Spark-Ignition Engine," SAE Technical Paper 2004-01-1915, 2004, doi:10.4271/2004-01-1915.
16. Santoso, H. and Cheng, W., "Mixture Preparation and Hydrocarbon Emissions Behaviors in the First Cycle of SI Engine Cranking," SAE Technical Paper 2002-01-2805, 2002, doi:10.4271/2002-01-2805.
17. Klein, D. and Cheng, W., "Spark Ignition Engine Hydrocarbon Emissions Behaviors in Stopping and Restarting," SAE Technical Paper 2002-01-2804, 2002, doi:10.4271/2002-01-2804.
18. Cheng, Wai K., and Fuquan Zhao. "Transient Engine Startup and Shutdown Processes." In Technologies for Near-Zero-Emission Gasoline-Powered Vehicles, 1–29. SAE International, ISBN 978-0768014617, 2007.
19. Cambustion. "Gasoline Direct Injection Particulate Measurement with the DMS Series". Application Note DMS08.
20. Eiglmeier, C., B. Pfalzgraf, J. Helbig, S. Adam, M. Grigo, R. Dornhöfer, and A. Eiser. "Der Neue R4 – 2,0l TFSI SULEV/PZEV-Motor von Audi." In , 16. Aachener Kolloquium Fahrzeug- und Motorentechnik, 2007.
21. Kudo, H., I. Hirose, T. Kihara, M. Yamakawa, and M. Hitomi. "MAZDA SKYACTIV-G 2.0L Gasoline Engine." In , 20th Aachen Colloquium Automobile and Engine Technology, 2011.

22. Kufferath, Andreas, Wolfgang Samenfink, and Jürgen Gerhardt. "Die neue Emissionsstrategie der Benzin-Direkteinspritzung." *MTZ - Motortechnische Zeitschrift*, Nov. 2003, doi:10.1007/BF03227138.
23. Eng, J., "The Effect of Spark Retard on Engine-out Hydrocarbon Emissions," SAE Technical Paper 2005-01-3867, 2005, doi:10.4271/2005-01-3867.
24. Cedrone, K. and Cheng, W., "SI Engine Control in the Cold-Fast-Idle Period for Low HC Emissions and Fast Catalyst Light Off," *SAE Int. J. Engines* 7(2):968-976, 2014, doi:10.4271/2014-01-1366.
25. Cedrone, K. and Cheng, W., "Using Valve Timing and Exhaust Back Pressure to Improve Catalyst Warm-Up Time," SAE Technical Paper 2013-01-2656, 2013, doi:10.4271/2013-01-2656
26. Rodríguez, J. Felipe, and Wai K. Cheng. "Fuel Accounting for the First Cranking Cycle of a GDI Engine." In *THIESEL 8th International Conference on Thermo-and Fluid Dynamic Processes in Direct Injection Engines*. Valencia, Spain, 2014.
27. Heywood, John B. "Internal Combustion Engine Fundamentals". New York, McGraw-Hill, 1988. ISBN 978-0070286375
28. Cheng, W., Hamrin, D., Heywood, J., Hochgreb, S. et al., "An Overview of Hydrocarbon Emissions Mechanisms in Spark-Ignition Engines," SAE Technical Paper 932708, 1993, doi:10.4271/932708.
29. Ketterer, J. and Cheng, W., "On the Nature of Particulate Emissions from DISI Engines at Cold-Fast-Idle," *SAE Int. J. Engines* 7(2):986-994, 2014, doi:10.4271/2014-01-1368.
30. Hoffmann, G., Befrui, B., Berndorfer, A., Piock, W. et al., "Fuel System Pressure Increase for Enhanced Performance of GDI Multi-Hole Injection Systems," *SAE Int. J. Engines* 7(1):519-527, 2014, doi:10.4271/2014-01-1209.
31. Burke, D., Foti, D., Haller, J., and Fedor, W., "Fuel Rail Pressure Rise during Cold Start of a Gasoline Direct Injection Engine," SAE Technical Paper 2012-01-0393, 2012, doi:10.4271/2012-01-0393.

Contact Information

Felipe Rodríguez, jfrb@mit.edu

Wai Cheng, wkcheng@mit.edu

Acknowledgments

The authors would like to acknowledge the support for this research by Borg-Warner, Chrysler, Ford Motor Company, and General Motors Company through a Consortium on Engine and Fuels Research.

Definitions/Abbreviations

AFR	Air Fuel Ratio	ρ_{std}	Exhaust density at standard pressure and temperature
aTDC-c	After Top Dead Center Compression	scc	Standard Cubic Centimeter
aTDC-i	After Top Dead Center Intake	SOI	Start of Injection
BDC	Bottom Dead Center	TDC	Top Dead Center
CMD	Count Median Diameter	$\tau(t)$	Time correction due to transit and response times
D_p	Particle diameter	\hat{x}_k	Mole fraction of species “k”
FEF	Fuel Enrichment Factor		
η_{vol}	Volumetric efficiency		
EVC	Exhaust Valve Closing		
EVO	Exhaust Valve Opening		
γ	Heat capacity ratio		
GDI	Gasoline Direct Injection		
IVC	Intake Valve Closing		
IVO	Intake Valve Opening		
\hat{M}	Particle mass concentration per scc		
MAP	Manifold Absolute Pressure		
MBT	Maximum Brake Torque		
M_{exh}	Exhaust molecular weight		
$m_{f,cyl}$	Injected mass of fuel per cylinder		
$m_{k,cycle}$	Mass emissions of species “k”		
M_k	Molecular weight of species “k”		
MFB	Mass Fraction Burned		
\hat{N}	Particle number concentration per scc		
PFI	Port Fuel Injection		
PMP	Particle Measurement Program		
ρ_{int}	Intake manifold air density		